2006

Reduction behavior of potassium-promoted iron oxide under mixed steam/hydrogen atmospheres

Sipho C. Ndlela
Iowa State University

Brent H. Shanks
Iowa State University, bshanks@iastate.edu

Reduction behavior of potassium-promoted iron oxide under mixed steam/hydrogen atmospheres

Abstract
Potassium-promoted iron oxide catalysts are used in large volume for the commercial ethylbenzene dehydrogenation to styrene process. Short-term deactivation of these catalysts, which is addressed by operating in excess steam, is thought to be caused due to reactive site loss through coking and/or reduction. However, the relative importance of the two mechanisms is not known. Presented are results concerning the reduction behavior of potassium-promoted iron oxide materials in the absence of carbon. Thermogravimetric experiments and X-ray diffraction analysis were used to examine the reduction behavior of potassium-promoted iron oxide materials. The reduction behavior was then compared with results from isothermal ethylbenzene dehydrogenation reactor studies under low steam-to-ethylbenzene operation. Potassium incorporation was found to stabilize the iron oxide against reduction apparently through the formation of KFeO 2. Chromium addition improved the reduction resistance, which gave good qualitative agreement with the dehydrogenation reaction studies. In contrast, vanadium incorporation led to more significant reduction as well as poor stability in the dehydrogenation reaction.

Keywords
dehydrogenation reactors, coking, dehydrogenation, potassium, reduction, iron oxides, potassium, x ray diffraction analysis

Disciplines
Biological Engineering | Chemical Engineering

Comments
Reprinted (adapted) with permission from *Industrial and Engineering Chemistry Research* 45 (2006): 7427, doi: 10.1021/ie0605229.

Reduction Behavior of Potassium-Promoted Iron Oxide under Mixed Steam/Hydrogen Atmospheres

Sipho C. Ndlela and Brent H. Shanks*

Department of Chemical and Biological Engineering, 2114 Sweeney Hall, Iowa State University, Ames, Iowa 50011-2230

Potassium-promoted iron oxide catalysts are used in large volume for the commercial ethylbenzene dehydrogenation to styrene process. Short-term deactivation of these catalysts, which is addressed by operating in excess steam, is thought to be caused due to reactive site loss through coking and/or reduction. However, the relative importance of the two mechanisms is not known. Presented are results concerning the reduction behavior of potassium-promoted iron oxide materials in the absence of carbon. Thermogravimetric experiments and X-ray diffraction analysis were used to examine the reduction behavior of potassium-promoted iron oxide materials. The reduction behavior was then compared with results from isothermal ethylbenzene dehydrogenation reactor studies under low steam-to-ethylbenzene operation. Potassium incorporation was found to stabilize the iron oxide against reduction apparently through the formation of $KFeO_2$. Chromium addition improved the reduction resistance, which gave good qualitative agreement with the dehydrogenation reaction studies. In contrast, vanadium incorporation led to more significant reduction as well as poor stability in the dehydrogenation reaction.

Introduction

Commercially, ethylbenzene (EB) dehydrogenation to styrene (ST) is predominantly performed using potassium-promoted iron oxide catalysts. This dehydrogenation reaction is operated in the presence of excess steam largely due to a significant loss in catalyst activity when steam-to-ethylbenzene molar ratios (S/EB) of less than 8 are used rather than the more commercially common S/EB of 8−10. It is economically desirable to operate at a lower S/EB where the activity constraint is due to the thermodynamics of the reversible dehydrogenation reaction rather than the catalyst activity requirement. The extent to which short-term deactivation of potassium promoted iron oxide catalysts occurs upon reduction of the S/EB has been shown previously.[1,2] The loss in activity associated with operating at decreasing S/EB has been historically ascribed to active site blockage due to catalyst coking.[3−8]

While K was originally added as a promoter to enhance the rate of carbon gasification from the iron oxide catalyst,[4−12] K was found to enhance the performance of the iron oxide catalyst even when carbon was not present on the catalyst, which led to more extensive studies on the interaction between the K promoter and the iron oxide.[4,7,10−19] It is now generally accepted that potassium monoferrite ($KFeO_2$), which resides on the surface of a bulk magnetite phase (Fe_3O_4) under reaction conditions, is the active site for the K-promoted iron oxide dehydrogenation catalysts.[7,17,20,21] Therefore, maintenance of the $KFeO_2$ phase at the catalyst surface is necessary to keep the catalyst in an active state. Muhler et al.[21] suggested that $KFeO_2$ is maintained over the life of the catalyst through a supply of K ions stored in a potassium polyferrite phase ($K_2Fe_{22}O_{34}$). This $K_2Fe_{22}O_{34}$ phase has been speculated to be intergrown with Fe_3O_4 in the bulk of catalyst under reaction conditions.[18−24]

The presence of the $KFeO_2$ phase at the catalyst surface during reaction necessitates having Fe^{3+} at the surface. When the S/EB is decreased, the reaction environment becomes more reductive, which could result in reduction of the surface Fe causing a loss of active sites. It is therefore possible that catalyst deactivation due to low S/EB can be influenced by loss of active sites through either blockage by carbon or Fe reduction.[5,6,20−22] To design dehydrogenation catalysts that can operate at lower S/EB, understanding the relative importance of these two deactivation mechanisms is important.

Since the manifestation of either deactivation mechanism is the loss of active sites, experiments need to be designed to decouple the two mechanisms to validate their importance in the deactivation behavior observed at low S/EB. A previous study examined the reduction behavior of K-promoted iron oxide in the presence of promoters that were historically used in EB dehydrogenation catalysts.[1] The reduction experiments in the study, which were analyzed using thermogravimetry and X-ray diffraction, were performed using low hydrogen partial pressure (0.003 atm) in a nitrogen atmosphere. The results from the study as well as a previous study by Muhler et al.[21] demonstrated that the inclusion of promoters influenced the reduction properties of the iron oxide. However, the change in reduction properties of the promoted iron oxide materials did not correlate with the expected performance of the materials under low S/EB reaction conditions.

A possible limitation of the previous studies was the reduction atmosphere used. The thermogravimetry studies used a nitrogen atmosphere containing only hydrogen, which contrasts significantly with the hydrocarbon/steam/hydrogen environment present during the dehydrogenation reaction in a reactor system. The need to exclude hydrocarbons from the reduction study due to the potential complications of coking still leaves a steam/hydrogen environment that might be more representative of the reduction conditions in the reaction system.

Previous studies have examined the reduction of iron oxide to iron metal under steam/hydrogen atmospheres.[25−30] It is clear from these studies that the presence of steam in the gas atmosphere significantly affected the reduction behavior. However, these studies did not address the impact of steam presence

* To whom correspondence should be addressed. Tel.: (515) 294-1895. Fax: (515) 294-2689. E-mail: bshanks@iastate.edu.

10.1021/ie0605229 CCC: $33.50
Published on Web 09/21/2006

Table 1. Compositions of the Materials Synthesized for the TGA Studies

	Metal Oxide/Carbonate Promoter (wt %)					(wt %)		
name	α-Fe_2O_3	K_2CO_3	Cr_2O_3	V_2O_5	K_2CrO_4	K	Cr	V
Fe_2O_3	100							
Fe_2O_3 w/Cr	93		7				5	
Fe_2O_3 w/V	91			9				5
K−Fe_2O_3	82	18				10		
K−Fe_2O_3 w/Cr	75	18	7			10	5	
K−Fe_2O_3 w/Cr	77	4			19	10	5	
K−Fe_2O_3 w/V	73	18		9		10		5
$KFeO_2$	47	53				30		

on the partial reduction of Fe_2O_3 to Fe_3O_4, which is the reduction of interest with the ethylbenzene dehydrogenation catalyst.

To examine the influence of a mixed steam/hydrogen environment on the partial reduction of iron oxide, the thermogravimetric analysis (TGA) approach used previously with only the hydrogen reductant[1] was extended in the current work to examine reduction behavior when iron oxide and promoted iron oxide was exposed to a mixed steam/hydrogen atmosphere. In addition to the TGA studies, isothermal ethylbenzene dehydrogenation reactor studies were performed using the same promoted iron oxide compositions examined using TGA. The reaction studies were conducted at low S/EB ratio to compare the catalytic performance of the materials to their reduction behavior.

Experimental Section

TGA Sample Preparation. The materials used in the experiments were iron oxide (α-Fe_2O_3), potassium carbonate (K_2CO_3), chromium oxide (Cr_2O_3), vanadium pentoxide (V_2O_5), potassium chromate K_2CrO_4, and potassium dichromate K_2CrO_7, which were provided by Shell Chemical Co. For materials made with K_2CrO_4 or K_2CrO_7 all of the Cr came from the mixed oxide, and the balance of the K from K_2CO_3. Detailed preparation and synthesis of powder samples were discussed previously.[1] Table 1 gives the promotion levels for each catalyst system where the compositions are based on precalcination, e.g., K_2CO_3 rather than K_2O. Samples were mixed and then calcined at either 800 or 950 °C for 3.5 h in a tube furnace under flowing air. Synthetic $KFeO_2$ was prepared with a potassium level of 30 wt % using a preparation temperature of 800 °C in flowing air.

Sample Characterization and TGA Studies. Surface areas were measured using a Micromeritics ASAP 2000 Brunauer−Emmett−Teller (BET) physisorption apparatus with krypton as the adsorbing gas. XRD characterization was performed using a Siemens D 500 X-ray diffractometer with a Cu Kα radiation source. The iron oxide samples upon removal from the TGA were stored under ultrahigh pure nitrogen, and the XRD analysis was performed within 24 h of removal from the TGA. TGA experiments used a Perkin-Elmer TGA 7. In the TGA reaction chamber, the inlet H_2 partial pressure (p_{H_2}) was 0.057 atm with a total gas flowrate of 70 mL/min. Before the start of the TGA experiments, the sample was heated in ultrahigh purity N_2 from 50 to 630 °C at 40 °C/min. Following heating in nitrogen, TGA isothermal experiments were performed at 630 °C for 360 min with $p_{H_2} = 0.057$ atm and variable steam concentrations. Steam to hydrogen mole ratios (S/H_2) ranged from 0.44 to 0.076. The 360 min run period run was divided into 6 time intervals each with a diminishing S/H_2. The first time interval was a 55 min period (at $S/H_2 = 0.44$) followed by a 5 min period for equilibration at the next S/H_2 step condition. Therefore, the second time interval was from 55 to 115 min ($S/H_2 = 0.29$), the third interval was from 115 to 175 min ($S/H_2 = 0.21$), the fourth interval was from 175 to 235 min ($S/H_2 = 0.15$), the fifth interval was from 235 to 295 min ($S/H_2 = 0.10$), and the final interval was from 295 to 360 min. ($S/H_2 = 0.076$). The isothermal temperature was selected due to its commercial relevance.

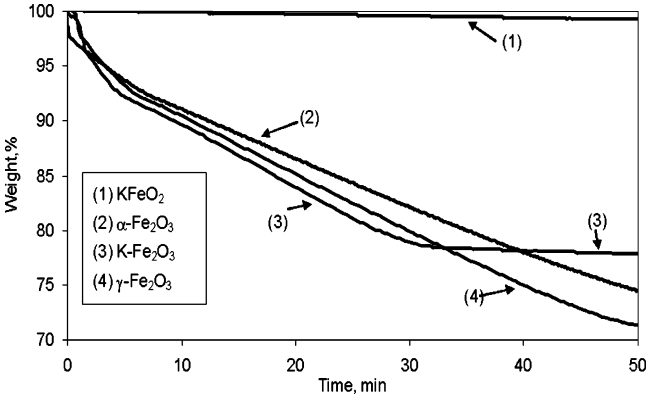

Figure 1. TG curves for the Fe_2O_3 materials reduced at 630 °C and $p_{H_2} = 0.057$ atm.

Isothermal Reactor Studies. Catalyst pellets were prepared by mixing iron oxide with similar promoters and promoter levels as discussed above in Table 1. The formulations used in the reactor studies were K−Fe_2O_3 with Cr (either Cr_2O_3 or K_2CrO_4) or V (V_2O_5). The formed catalyst pellets, which were 3.2 mm in diameter and 5 mm in length, were split into two sets and calcined at 800 and 950 °C, respectively. The catalyst samples were then tested in an isothermal reactor system that used metered liquid pumps to supply the ethylbezene and water, which were subsequently vaporized prior to introduction to the reactor. The 2.6 cm inner diameter reactor was loaded with 100 cm^3 of catalyst giving a bed length of 16 cm. The isothermal studies were performed at a catalyst bed temperature of 600 °C and pressure of 0.75 atm. During the experiments, the ethylbenzene flow rate was held constant at 0.009 mol/min while the steam flow rate was stepwise decreased from 0.106 to 0.044 mol/min, which corresponded to a steam to ethylbenzene mole ratio (S/EB) from 12 to 5. The reactor effluent stream was analyzed using a HP 5890 series II gas chromatograph equipped with a FID detector and a J&M Scientific DB-Wax column.

Results and Discussion

Isothermal H_2 TGA Experiments. To provide a basis for the steam−H_2 work, 630 °C isothermal TGA experiments were performed in a hydrogen only environment with a partial pressure of $p_{H_2} = 0.057$ atm. Shown in Figure 1 are the thermogravimetric (TG) curves for several of the samples. Under these conditions, the total weight loss was both the highest and similar for the hematite (α-Fe_2O_3) and maghemite (γ-Fe_2O_3) samples, whereas the K−Fe_2O_3 had a slightly lower weight loss. In contrast, $KFeO_2$ was resistant to the reductive atmosphere and gave no weight loss or concomitant phase change throughout the entire experiment. The weight loss for α-Fe_2O_3 and γ-Fe_2O_3 was monotonic through the experiment, so that discrete changes in iron oxide phases were not evident.

For all of the samples other than $KFeO_2$, a series of TGA runs were terminated at 5, 10, and 50 min and the resulting materials analyzed using XRD. After 5 min under the reductive conditions, α-Fe_2O_3 had transformed to a mixture of α-Fe_2O_3

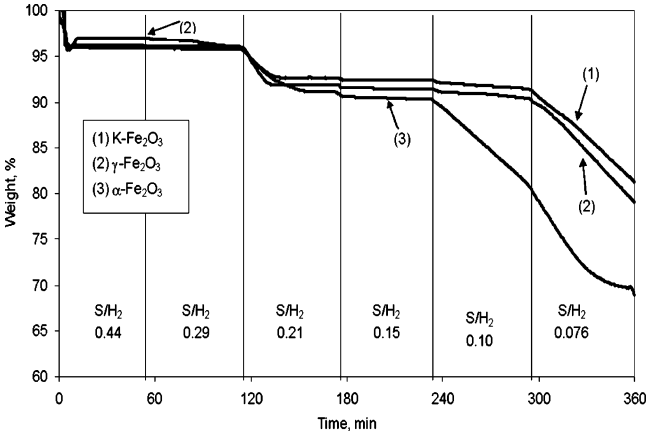

Figure 2. TG curves for Fe_2O_3 materials at 630 °C and mixed S/H_2 with $p_{H_2} = 0.057$ atm.

and γ-Fe_2O_3 and at the 10 min point was a mixture of α-Fe_2O_3, γ-Fe_2O_3, and magnetite (Fe_3O_4). The successive reduction of α-Fe_2O_3 to Fe_3O_4 through the intermediate γ-Fe_2O_3 in a hydrogen atmosphere has been reported previously.[31,32] This progression occurs since α-Fe_2O_3 first transforms to the cubic crystal structure of γ-Fe_2O_3, which can be subsequently reduced to the similar cubic crystal structure of Fe_3O_4. After 50 min in the reductive atmosphere for the α-Fe_2O_3 sample, the three iron oxide phases were still present, but a significant amount of fully reduced iron (Fe) was also observed. The FeO phase was not observed in any of the samples. Despite being an intermediate phase in the reduction of α-Fe_2O_3 to Fe_3O_4. The γ-Fe_2O_3 appeared to yield a weight loss trajectory similar to that for α-Fe_2O_3 in the reduction experiments.

The only crystalline phase present in the K$-$$Fe_2O_3$ sample prior to the reduction experiment, as determined by XRD analysis, was α-Fe_2O_3. However, when exposed to the hydrogen atmosphere for only 5 min, the only crystalline phases present were γ-Fe_2O_3 and $KFeO_2$. The rapid transformation to γ-Fe_2O_3 with this sample suggests that the presence of potassium facilitates the transformation of the iron oxide from α-Fe_2O_3 to γ-Fe_2O_3. When the K$-$$Fe_2O_3$ sample was only exposed to ultrahigh purity nitrogen at 630 °C for 5 min, no transformation from the initial α-Fe_2O_3 was observed indicating that the presence of hydrogen did facilitate the transformation from α-Fe_2O_3 to γ-Fe_2O_3 as well as the formation of $KFeO_2$. When the sample was exposed to the reductive atmosphere for 10 min, the γ-Fe_2O_3, Fe_3O_4, and $KFeO_2$ phases were observed. As can be seen in Figure 1, the weight loss curve for the K$-$$Fe_2O_3$ sample departed from that of the two pure iron oxide samples at 30 min. Similarly to the iron oxide samples, the K$-$$Fe_2O_3$ sample upon reduction for 50 min was found to contain γ-Fe_2O_3, Fe_3O_4, and Fe. However, the presence of $KFeO_2$ was also observed, so the attenuation of weight loss observed for the K$-$$Fe_2O_3$ sample would appear to be due to the partial formation of this more stable phase.

Isothermal Steam$-$$H_2$ TGA Experiments. To determine the influence of a mixed steam$-$hydrogen (S/H_2) atmosphere on the iron oxide systems, TGA experiments were performed at 630 °C and $p_{H_2} = 0.057$ atm using S/H_2 ranging from 0.44 to 0.076. Shown in Figure 2 are the TG curves for α-Fe_2O_3, γ-Fe_2O_3, and K$-$$Fe_2O_3$ under the conditions imposed in the S/H_2 experiments. The weight losses seen within the initial 5 min are associated with equilibration disturbances that include thermal effects, gas transport, and mechanical variation weighing mechanism.[1] At the end of the first S/H_2 condition, the α-Fe_2O_3 and γ-Fe_2O_3 samples were observed from XRD to still only contain the same phase as their respective initial samples. In contrast, the K$-$$Fe_2O_3$ sample, which gave only the α-Fe_2O_3 phase in the initial sample, had partially transformed such that the γ-Fe_2O_3 phase was present.

As discussed above in the hydrogen-only experiments, the introduction of K to α-Fe_2O_3 in making the K$-$$Fe_2O_3$ sample led to a material that more readily transformed to γ-Fe_2O_3 in the presence of hydrogen. This transformation also occurred in the S/H_2 experiments. To determine whether the presence of hydrogen was essential for this transformation, K$-$$Fe_2O_3$ samples were subjected to either ultrahigh purity nitrogen or nitrogen with steam at 630 °C. In both cases no formation of the γ-Fe_2O_3 phase was observed by XRD. Therefore, the presence of both hydrogen and K was required to facilitate the formation of the cubic γ-Fe_2O_3 phase.

As the samples were exposed to lower S/H_2 conditions, the samples were found to contain mixed iron oxide phases. To better compare the transformation of the samples, a method was employed to quantify the amount of each phase observed by XRD.[33−36] The quantitative XRD method used was the internal standard method, which was developed by Klug and Alexander and has been successfully applied to a number of mixed phase systems.[33−37] The internal standard method uses the ratio of peak intensities to quantify the amount of each phase. The key assumptions for the Klug and Alexander equation are that the samples are homogeneous, flat, and infinitely thick, have consistent particle sizes compared to other samples tested, are randomly orientated with no preferred orientation, and have a change in d spacing that is constant for all samples and that the incident beam is intercepted by the sample at all Bragg angles.[34] These assumptions were reasonable for the samples used in this study.

This particular method, which is given in eq 1, is referred to as the relative intensity ratio method,

$$I_y = (M_y k_y)/(f_y u) \tag{1}$$

where, I_y is the intensity of the jth line of compound y, M_y is the weight fraction of y, f_y is the mass density of y, u is the mass absorption coefficient for the sample, and k_y is the constant for a given line of a given compound. To use eq 1, control samples (subscript c) were prepared that consisted of measured amounts of pure silicon (Si) mixed with pure α-Fe_2O_3, γ-Fe_2O_3, or Fe_3O_4. The equation then defining the relative intensity of the Si (I_{si}) to Fe_3O_4 (I_{Fe}) in a control sample is given by

$$\begin{aligned}(I_{Si}/I_{Fe})_c &= [(M_{Si}k_{si})/(f_{Si}u_c)]/[(M_{Fe}K_{Fe})/(f_{Fe}u_c)] \\ &= [(M_{Si}/M_{Fe})(k_{Si}/K_{Fe})(f_{Fe}/f_{Si})]_c \end{aligned} \tag{2}$$

with comparable expressions for the other iron oxide control samples. To quantify the multiple phases present in a tested TGA sample (subscript t), a measured amount of Si was mixed with a known amount of the tested sample, so that Si could be used as the internal standard. The amount of a specific phase present in the test sample was determined by referencing the test sample to the control sample for that phase. For example, the Fe_3O_4 content was determined using eqs 2 and 3.

$$\begin{aligned}(I_{si}/I_{Fe})_t &= [(M_{Si}k_{Si})/(f_{Si}u_t)]/[(M_{Fe}K_{Fe})/(f_{Fe}u_t)] \\ &= [(M_{Si}/M_{Fe})(k_{si}/K_{Fe})(f_{Fe}/f_{Si})]_t \end{aligned} \tag{3}$$

$$[(I_{Si}/I_{Fe})]_c/[(I_{Si}/I_{Fe})]_t = [(M_{Si}/M_{Fe})(k_{Si}/K_{Fe})(f_{Fe}/f_{Si})]_c/[(M_{Si}/M_{Fe})(k_{si}/K_{Fe})(f_{Fe}/f_{Si})]_t$$

$$[(I_{Si}/I_{Fe})]_c/[(I_{Si}/I_{Fe})]_t = [M_{Si}/M_{Fe}]_c/[M_{Si}/M_{Fe}]_t$$

$$(M_{Fe})_t = [(I_{si}/I_{Fe})_c(M_{Fe}/M_{si})_c](I_{Fe}/I_{si})_c(M_{si})_t \quad (4)$$

Subsequently, the normalized value for the Fe_3O_4 fraction (M_{NFe}) in the tested sample was obtained by taking into consideration the dilution factor resulting from mixing in the Si internal standard as given in

$$(M_{NFe})_t = (M_{Fe})_t/[1 - (M_{Si})_t] \quad (5)$$

The final normalized fractional weight of Fe_3O_4 was obtained by substituting eq 4 into eq 5:

$$(M_{NFe})_t = [(I_{Si}/I_{Fe})_c(M_{Fe}/M_{Si})_c](I_{Fe}/I_{Si})_c(M_{Si})_t/[1 - (M_{Si})_t] = Z(I_{Fe}/I_{Si})_c(M_{Si})_t/[1 - (M_{Si})_t] \quad (6)$$

The Z term was determined by taking the XRD intensity ratio with the Fe_3O_4 control sample. For the quantification, the peaks selected for the peak intensity ratios were 2θ angles of 28.442° for silicon and 33.152, 35.630, and 35.422° for α-Fe_2O_3, γ-Fe_2O_3, or Fe_3O_4, respectively, which correspond to the highest intensity peak for each phase. Selection of the highest intensity peak for each component created an issue of overlap between the γ-Fe_2O_3 (35.630°) and Fe_3O_4 (35.422°) peak. Increasing the scan time from 2 to 3 s decreased the extent of the overlap. In addition, decomposition of the overlapping peaks was performed by overlaying the relevant control samples on the tested TGA sample. More complete details of the procedure used can be found elsewhere.[38]

Shown in Figure 3a,b are example XRD patterns for α-Fe_2O_3 and K$-$$Fe_2O_3$ samples that had been run in the TGA experiments with the S/H_2 atmosphere for 295 min corresponding to a final S/H_2 of 0.10. The individual phase identification was confirmed with the relevant powder diffraction (PDF) cards. The numbers of the PDF cards that were used are given in the legend of the figures. The results of the quantification of the crystalline phases present in these samples as well as samples taken at different S/H_2 conditions are given in Tables 2 and 3.

Table 2 gives the reduction evolution of the α-Fe_2O_3 sample as the S/H_2 is decreased, which can be compared with the coupled TGA data for this sample (Figure 2). No phase transformation was observed for the α-Fe_2O_3 sample until the S/H_2 was decreased below 0.15. The weight loss seen upon decreasing the S/H_2 from 0.29 to 0.15 did not appear to be associated with a reduction in the iron oxide. It is possible that the weight change was due to loss of surface hydroxyl groups on the iron oxide as several studies have suggested the presence of these groups on iron oxide surfaces.[21] Once the S/H_2 was decreased to 0.10, significant reduction began to occur. The sample had not reached a steady-state condition after 60 min at this S/H_2 value. However, the clear transformation of α-$Fe_2O_3 \rightarrow \gamma$-$Fe_2O_3 \rightarrow Fe_3O_4 \rightarrow$ Fe can be seen. The reduction is likely occurring from the outer portion of the iron oxide particle into its core. The simultaneous presence of α-Fe_2O_3 and Fe indicates that the reduction of the interior of the particle is limited by diffusion of hydrogen and that the rate of reduction at the surface is faster than this diffusion process.

Table 2. XRD Analysis Data for Unpromoted Iron Oxide TGA Samples

S/H_2 molar ratio (sample time, min)	α-Fe_2O_3 (wt %)	γ-Fe_2O_3 (wt %)	Fe_3O_4 (wt %)	Fe (wt %)
0.15 (235)	100	0	0	0
0.10 (295)	19	18	20	43
0.076 (360)	8	17	13	62

Table 3. XRD Analysis Data for K$-$$Fe_2O_3$ TGA Samples

S/H_2 molar ratio (sample time, min)	γ-Fe_2O_3 (wt %)	Fe_3O_4 (wt %)	Fe (wt %)	$KFeO_2$ (wt %)
0.21 (175)	89	11	0	0
0.15 (235)	62	38	0	0
0.10 (295)	35	11	35	19
0.076 (360)	32	14	51	3

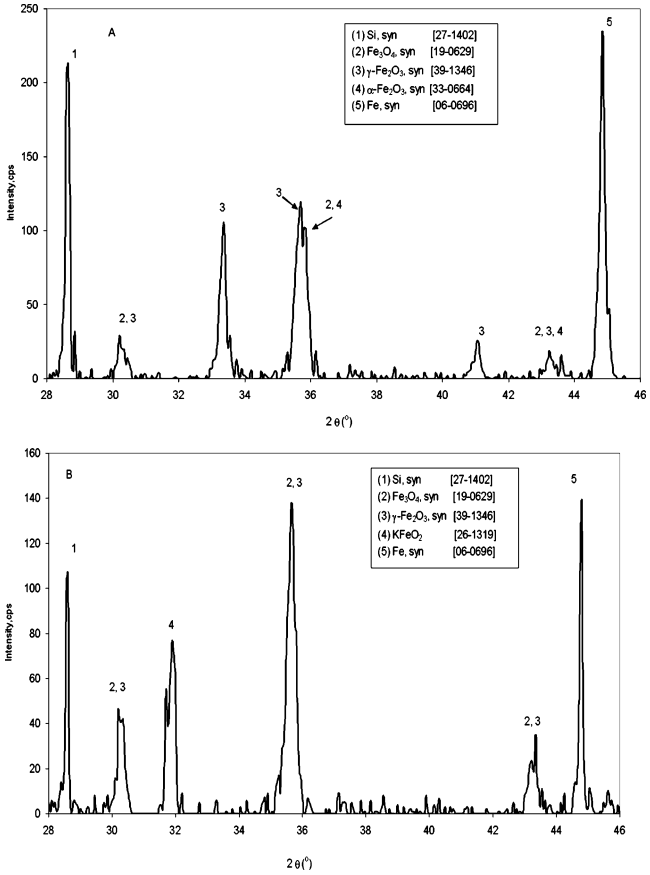

Figure 3. (a) XRD data for α-Fe_2O_3 removed after exposure to $S/H_2 = 0.10$. (b) XRD data for K$-$$Fe_2O_3$ removed after exposure to $S/H_2 = 0.10$.

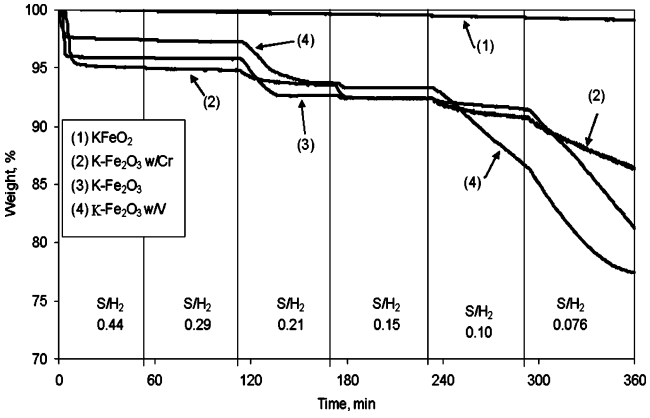

Figure 4. TG curves for copromoted Fe_2O_3 materials at mixed steam/H_2 conditions.

The quantified XRD data and TGA curve for the K$-$$Fe_2O_3$ sample are given in Table 3 and Figure 4. Introduction of K to the iron oxide facilitated the transformation of the iron oxide from α-Fe_2O_3 to γ-Fe_2O_3 as the presence of both γ-Fe_2O_3 and Fe_3O_4 was already observed at the S/H_2 value of 0.21. This

Table 4. XRD Data Analysis for K−Fe_2O_3 w/V TGA Samples

S/H_2 molar ratio (sample time, min)	γ-Fe_2O_3 (wt %)	Fe_3O_4 (wt %)	Fe (wt %)	$KFeO_2$ (wt %)
0.15 (240)	58	42	0	0
0.10 (300)	20	20	60	0
0.076 (360)	15	7	78	0

behavior was in marked contrast to the pure α-Fe_2O_3 sample, which did not begin to transform to γ-Fe_2O_3 and reduce to Fe_3O_4 until a lower S/H_2 condition. The enhanced formation of γ-Fe_2O_3 in the K−Fe_2O_3 sample and the role of γ-Fe_2O_3 as an intermediate in the reduction of α-Fe_2O_3 to Fe_3O_4 led to more facile reduction to a lower iron oxidation state. Therefore, the reduction behavior of K−Fe_2O_3 was significantly different from that for α-Fe_2O_3, which can be seen from their TGA curves and XRD data. While reduction initiated at a higher S/H_2 condition for the K−Fe_2O_3 sample, the overall amount of reduction for this sample was lower than for the α-Fe_2O_3 sample and formation of the $KFeO_2$ phase was observed.

The formation of $KFeO_2$ during the reduction of K−Fe_2O_3 would appear to contribute significantly to the reduction behavior of K−Fe_2O_3. As discussed previously and shown in Figure 4, the ex situ synthesized $KFeO_2$ material, which was olive green in color, was found to not reduce under any of the S/H_2 conditions imposed in the TGA experiment and in fact was not reduced by hydrogen even in the absence of steam (Figure 1). The in situ formation of the $KFeO_2$ phase during the TGA experiment then is likely the cause of the increased reduction stability of K−Fe_2O_3 relative to α-Fe_2O_3 and the suppression of reduction all the way to Fe metal, which was observed for the α-Fe_2O_3 sample. This in situ $KFeO_2$ formation was reported previously for TGA reduction experiments performed without the presence of steam.[1] The reduction suppression to Fe metal is likely due to fact that the $KFeO_2$ phase appears to form on the outside of the iron oxide particles as demonstrated by the particles turning to an olive green color, which is consistent with the color of this potassium ferrite. It is important to note that the in situ formation of $KFeO_2$ did not occur until the S/H_2 was sufficiently low so as to cause some reduction of the iron oxide to Fe_3O_4. Therefore, the presence of Fe_3O_4 is necessary for the formation of $KFeO_2$ at the temperature used in the TGA study. The ex situ formation of $KFeO_2$ from α-Fe_2O_3 and K_2CO_3 in air required a temperature of 800 °C.

To further examine the impact of promoters on the reduction stability of iron oxide, samples of K−Fe_2O_3 additionally promoted with either Cr or V were also examined. In the ethylbenzene dehydrogenation reaction, the addition of Cr or V into potassium promoted iron oxide is known to impact the catalyst activity and selectivity.[6−9,12] Specifically, Cr has been described as a structural promoter for maintaining activity during low S/EB operation. In contrast, V promotion has been found to improve selectivity of dehydrogenation catalysts while negatively impacting catalyst activity during low S/EB operation.

The reduction behavior for K−Fe_2O_3 w/V is shown in Figure 4 for the TGA data and in Table 4 for the complementary XRD results. As can be seen in Figure 4, the weight loss over the course of the TGA experiment is larger for the K−Fe_2O_3 w/V sample than for the K−Fe_2O_3 sample. This difference can be attributed to the increased formation of the reduced Fe_3O_4 and Fe phases in the K−Fe_2O_3 w/V material. With K−Fe_2O_3 w/V, significant iron oxide reduction was already observed by the same 0.15 S/H_2 condition as was K−Fe_2O_3, but no measurable amount of the $KFeO_2$ was observed being formed during the reduction and more extensive reduction to Fe was observed.

Table 5. XRD Data Analysis for K−Fe_2O_3 w/Cr TGA Samples

S/H_2 molar ratio (sample time, min)	γ-Fe_2O_3 (wt %)	Fe_3O_4 (wt %)	Fe (wt %)	$KFeO_2$ (wt %)
0.21 (180 min)	100	0	0	0
0.15 (240 min)	100	0	0	0
0.10 (300 min)	100	0	0	0
0.076 (360 min)	53	38	9	0

Therefore, the incorporation of the V promoter into K−Fe_2O_3 suppresses the formation of $KFeO_2$, which appears to yield a material that is more readily reduced.

The influence of Cr promotion on the reduction behavior of K−Fe_2O_3 can be seen in Figure 4 (curve 2) and Table 5. This material had a lower overall weight loss than either K−Fe_2O_3 or K−Fe_2O_3 w/V in the TGA experiment. In addition, the XRD quantified reduction behavior was significantly different for the K−Fe_2O_3 w/Cr material. As shown in Table 5, the incorporation of Cr did not affect the iron oxide transformation from α-$Fe_2O_3 \rightarrow \gamma$-$Fe_2O_3$, but the further reduction of γ-Fe_2O_3 to Fe_3O_4 was significantly suppressed. The incorporation of Cr decreased the S/H_2 needed to cause reduction to 0.076, and at the end of the time period in which the sample was exposed to this low S/H_2 condition, only a small portion of the iron oxide had been completely reduced. The increase in reduction resistance under the isothermal steam−hydrogen TGA experiment that was observed with Cr promotion was in marked contrast to the hydrogen-only TGA reduction experiments reported previously.[1] In those previous TGA experiments, the K−Fe_2O_3 w/Cr material seemed to reduce more easily than either the K−Fe_2O_3 or K−Fe_2O_3 w/V material. Comparison of the results from the two different types of experiments further demonstrates the importance of including steam in the reduction experiments.

The results from the quantified XRD analysis for the K−Fe_2O_3 w/Cr material would suggest that the Cr interacts with the K thereby limiting the interaction of K with the iron oxide. In the absence of additional promoters, K was found to readily interact with α-Fe_2O_3 to facilitate its transformation to γ-Fe_2O_3 at the beginning of the TGA experiment, which was found to also be the case upon incorporation of Cr. Unlike with K−Fe_2O_3, the K−Fe_2O_3 w/Cr material did not have any measurable formation of the very stable $KFeO_2$ phase even after the TGA reduction had initiated.

Several studies have examined the phases that were formed when iron oxide was promoted with Cr and K. Plyasova et al.[39,40] and Andrushkevick et al.,[41] using XRD analysis and IR spectroscopy, reported a potassium chromate (K_2CrO_4) phase was formed on a model catalyst system consisting of an initial mixture of Fe_2O_3, K_2CO_3, and Cr_2O_3. In their studies the mixture was calcined above 600 °C in air, which resulted in a material containing the α-Fe_2O_3, $KFeO_2$, and K_2CrO_4 phases as well as a small amount of chromium oxide (Cr_2O_3). Under a reducing environment of either hydrocarbon/steam or hydrocarbon/hydrogen/steam, the K_2CrO_4 and Cr_2O_3 phases were no longer observed. The disappearance of these phases was speculated to have been caused by the decomposition/reduction of K_2CrO_4 to form amorphous Cr_2O_3 and K_2O.

To determine if the K/Cr interaction was critical in helping to stabilize the iron oxide against reduction, a sample was synthesized in which α-Fe_2O_3 and Cr_2O_3 were mixed and calcined at 800 °C. The resulting material gave a reduction performance in the S/H_2 TGA experiment similar to that seen for unpromoted α-Fe_2O_3, which was shown in Figure 2. Also, XRD analysis of the sample after exposure to an environment of $S/H_2 = 0.10$ resulted in mixed iron oxide phases similar to

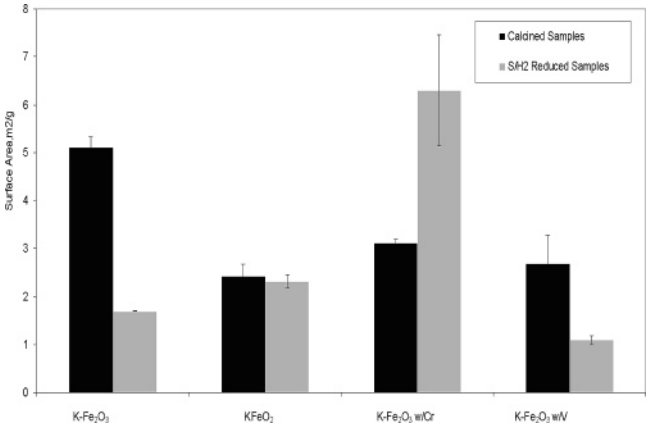

Figure 5. Sample surface areas after calcination at 800 °C and exposure to $S/H_2 = 0.076$.

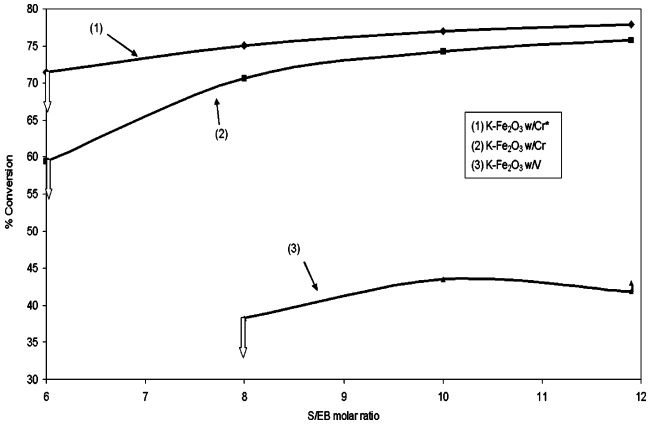

Figure 6. Conversion for decreasing S/EB ratios in an isothermal reactor (600 °C, 0.75 atm) with the arrows showing the point of stability loss. (The asterisk indicates Cr was added as K_2CrO_4.)

that reported in Table 2 for unpromoted α-Fe_2O_3. Therefore, it was apparent that Cr promotion alone could not impart reduction resistance to α-Fe_2O_3. It should be noted that this result was not unexpected since Cr−Fe phase formation requires calcination temperatures in excess of 1100 °C.[39]

The K−Fe_2O_3 sample used for the data in Figure 4 was promoted with 5 wt % Cr. The XRD analysis of this sample after calcination did not display the formation of any phases between K/Cr/Fe. To determine whether this result was due to the lack of phase formation or formation of a phase below the detection limit, a K−Fe_2O_3 sample was promoted with a higher Cr level of 10 wt %, while holding the K level at 10 wt %. Following calcination at 800 °C, the higher Cr-containing sample was found to have the presence of a K_2CrO_4 phase as well as α-Fe_2O_3. TGA testing of the K−Fe_2O_3 w/10 wt % Cr sample under the mixed S/H_2 conditions gave results similar to those shown in Figure 4 for the K−Fe_2O_3 w/5 wt % Cr material. The K_2CrO_4 phase was found to persist until the S/H_2 was reduced to 0.10 at which point the presence of the K_2CrO_4 phase decreased markedly along with the transformation of γ-Fe_2O_3 to the Fe_3O_4 phase.

The decomposition of the K_2CrO_4 phase in the absence of iron oxide was examined. A synthetic K_2CrO_4 material was subjected to the standard S/H_2 test, and the initiation of phase decomposition was observed when the S/H_2 was reduced to 0.21. Therefore, the K_2CrO_4 phase was stabilized against reduction by the presence of the iron oxide just as the α-Fe_2O_3 phase had been stabilized against reduction by K_2CrO_4.

To further examine the role of K_2CrO_4 in the mixed oxide system, a sample was prepared by mixing a pure K_2CrO_4 powder with α-Fe_2O_3 such that the 5 wt % Cr level in the resulting mixture was the same as that used in the synthesis of K−Fe_2O_3 w/Cr. TGA results for this K−Fe_2O_3 w/K_2CrO_4 system were then compared to the standard K−Fe_2O_3 w/Cr. No significant difference in weight loss behavior was observed for the samples indicating that the preformation of the K_2CrO_4 phase did not significantly change the reduction behavior relative to K−Fe_2O_3 w/Cr.

Surface Area Analysis. The hold time at each S/H_2 value during the TGA experiments was selected to achieve a stable weight value before a further decrease in the S/H_2, with the exception of S/H_2 values less than 0.10. However, due to the transient nature of the TGA experiments, it was important to determine if significant surface area differences were observed between the samples, which could contribute to the reduction results. The results from BET analysis of the samples before and after the TGA experiments are shown in Figure 5.

As can be seen from the figure, the starting surface areas for the materials were quite similar except for the K−Fe_2O_3 material, which had a slightly higher measured surface area. The surface areas for all of the samples decreased following the TGA experiment with the exception of the K−Fe_2O_3 w/Cr sample, which gave an increase in surface area. While the lowest surface area material, which was $KFeO_2$, was also the most stable, the K−Fe_2O_3 w/Cr sample, which had the highest surface area at the end of the TGA run, was the second most stable material. As such, the data do not support a correlation between surface area and sample stability thereby supporting the discussion that promoter interaction with the iron oxide is the critical factor in determining the resulting reduction stability behavior.

Isothermal Reactor Studies. Since a clear distinction in the reduction behavior of the tested samples were observed in the S/H_2 TGA experiments, the goal was to determine whether these differences translated to differences in performance under dehydrogenation reaction conditions in which hydrocarbons were also present. To examine the performance of the materials under reaction conditions, three model catalyst systems were used, K−Fe_2O_3 promoted with V (V_2O_5) or Cr (Cr_2O_3, K_2CrO_4). For the dehydrogenation reaction studies, the isothermal reactor was maintained at 600 °C with an outlet pressure of 0.75 atm. The fresh catalyst was started up using a S/EB of 12 and was subsequently held at this condition for 4 days to reach a steady-state condition. The reactor was then maintained at the S/EB = 12 steady-state conditions for an additional 3−4 days to ensure that no loss in catalyst dehydrogenation activity was observed. The S/EB was then decreased incrementally from 12 to 6 in steps of 2 units while ensuring that steady conditions were attained before lowering the feed molar ratio.

Figure 6 compares the activity for the K−Fe_2O_3 w/V and Cr (Cr_2O_3, K_2CrO_4) catalysts. The conversion data point at each S/EB level represents the average steady state point at each level where conversion is defined as the mole percent of the EB fed into the reactor that was converted. For example, the conversion value at S/EB = 12 was the average of the steady-state conversion data from the 5th through the 8th day of operation.

As reported previously, Cr promotion led to a more active catalyst at the initial condition relative to the V promoted catalyst with EB conversions of 75% and 40%, respectively. The promotion of K−Fe_2O_3 with Cr using either Cr_2O_3 or K_2CrO_4 gave fairly similar activity levels for the S/EB range 12−8. The arrows in Figure 6 for each of the model catalysts represent the S/EB values in which the catalyst activity did not reach a stable value within 2 days of operation. The conversion point on the graph represents the initial conversion that was measured when

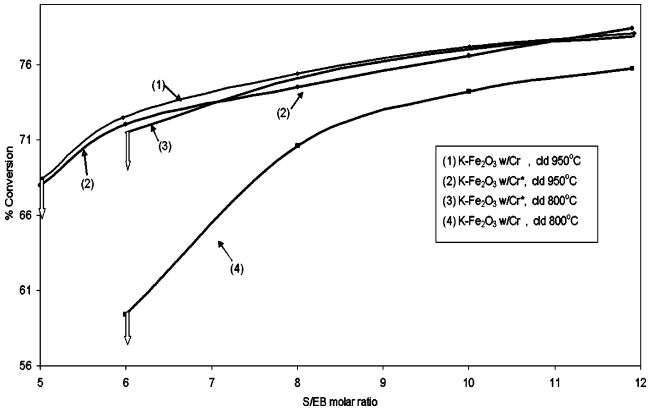

Figure 7. Effect of preparation calcination temperature on the isothermal performance of Cr-promoted $K-Fe_2O_3$. (The asterisk indicates Cr was added as K_2CrO_4.)

the S/EB was first lowered. Therefore, the $K-Fe_2O_3$ w/Cr catalysts were found to have stable conversion until the S/EB was lowered to 6, whereas the $K-Fe_2O_3$ w/V gave an unstable conversion when the S/EB was 8.

Qualitatively, the lower apparent stability with $K-Fe_2O_3$ w/V relative to $K-Fe_2O_3$ w/Cr was consistent with the results observed in the isothermal S/H_2 TGA experiments. It is important to note that this qualitative agreement does not allow the conclusion that a promoted $K-Fe_2O_3$ catalyst with better reduction resistance leads to a more stable catalyst under reaction conditions, since the current experiments do not provide insight to relative resistance of the $K-Fe_2O_3$ w/V and $K-Fe_2O_3$ w/Cr catalysts to formation of carbon on the catalyst surface.

A second set of $K-Fe_2O_3$ w/Cr catalysts made with either Cr_2O_3 or K_2CrO_4 were synthesized that were calcined at 950 °C instead of 800 °C. The reaction conversion results for these catalysts are given in Figure 7. As can be seen from the figure, the higher calcination temperature preparations led to catalysts with comparable initial activity to the lower calcination temperature material, but the S/EB level in which the catalysts became unstable was decreased to a S/EB of 5. If reduction resistance only was responsible for improved stability under reaction conditions, the higher calcinations temperature materials would be expected to demonstrate different behavior in the S/H_2 TGA experiments. These experiments were performed, but no difference in the isothermal S/H_2 TGA curves was observed for the 800 and 950 °C calcined materials. Therefore, the difference seen in the reactor studies for these materials did not translate to different reduction behavior in the TGA experiments.

Conclusions

The reduction behavior of K-promoted iron oxide under mixed S/H_2 atmospheres was found to be distinctly different than that reported previously in hydrogen-only reduction studies. The presence of hydrogen caused a rapid transformation from α-Fe_2O_3 to γ-Fe_2O_3 for the K-containing materials. This transformation was found to be facilitated by the presence of K as the unpromoted α-Fe_2O_3 did not readily change to the γ-Fe_2O_3 phase until further reduction to Fe_3O_4 was also observed. Preformed $KFeO_2$ was found to be stable even to the lowest S/H_2 conditions used in the study. In K-containing samples that did not initially have $KFeO_2$ present, the phase was found to form simultaneously with reduction of some of the iron oxide to Fe_3O_4, which could subsequently impart some reduction resistance to the partially reduced material. Copromotion of $K-Fe_2O_3$ with V led to a material that was more easily reduced than the $K-Fe_2O_3$ by itself. In contrast, the use of Cr as a copromoter improved the reduction resistance of the iron oxide, which apparently involved some interaction between the Cr and K. Isothermal reaction testing of the model copromoted iron oxide systems gave S/EB behavior consistent with the reduction resistance rank ordering found in the S/H_2 experiments. However, the isothermal S/EB reaction experiments did not agree with the S/H_2 reduction experiments when $K-Fe_2O_3$ w/Cr samples were prepared with different calcinations temperatures suggesting that the S/H_2 reduction experiments cannot uniformly be used as a surrogate for determining the performance of an iron oxide-based dehydrogenation catalyst at low S/EB.

Acknowledgment

We gratefully acknowledge Dr. Ruth Kowaleski, Shell Chemicals, for her assistance with the reactor studies. This work was supported by the Shell Oil Foundation through the Faculty Fellow program and by the CRI Catalyst Co.

Literature Cited

(1) Ndlela, S. C.; Shanks, B. H. Reducibility of potassium-promoted iron oxide under hydrogen conditions. *Ind. Eng. Chem. Res.* **2003**, *42*, 2112−2121.

(2) Bhat, Y. S. Kinetics of Dehydrogenation of ethylbenzene to styrene over a promoted iron oxide catalyst. *Indian Chem. Eng.* **1988**, *3*, 43−48.

(3) Matsui, J.; Sodesawa, T.; Nazaki, F. Influence of carbon dioxide addition upon decay of activity of a potassium-promoted iron oxide catalyst for dehydrogenation of ethylbenzene. *Appl. Catal.* **1991**, *67*, 179−188.

(4) Hirano, T. Active phase in potassium-promoted iron oxide for dehydrogenation of ethylbenzene. *Appl. Catal*. **1986**, *26*, 81−90.

(5) Devoldere, K.; Froment, G. Coke Formation and gasification in the catalytic dehydrogenation of ethylbenzene. *Ind. Eng. Chem. Res*. **1999**, *38*, 2626−2633.

(6) Coulter, K.; Goodman, D. W.; Moore, R. G. Kinetics of the dehydrogenation of ethylbenzene to styrene over unpromoted and K-promoted model iron oxide catalysts. *Catal. Lett*. **1995**, *31*, 1−8.

(7) Muhler, M.; Schlogl, R.; Ertl, G. The nature of the iron oxide based catalyst for the dehydrogenation of ethlybenzene to styrene 2. Surface chemistry of active phase. *J. Catal*. **1992**, *138*, 413−444.

(8) Rostrup-Nielsen, J. R. Coking on nickel catalysts for steam reforming of hydrocarbons. *J. Catal*. **1974**, *33*, 184−201.

(9) Meima, G.; Menon, R.; Govind, P. Catalyst deactivation phenomena in styrene production. *Appl. Catal., A* **2001**, *212*, 239−245.

(10) Kurs, C.; Arita, Y.; Weiss, W.; Schlögl, R. Understanding heterogeneous catalysis on an atomic scale: a combined surface and reactivity investigation for the dehydrogenation of ethylbenzene over iron oxide catalysts. *Top. Catal*. **2001**, *14* (1−4), 111−123.

(11) Carrazza, J.; Tysoe, W. T.; Heinemann, H.; Somorjai, G. A. Gasification of graphite with steam below 900 k catalyzed by a mixture of potassium hydroxide and transition metal oxide. *J. Catal*. **1985**, *96*, 234−242.

(12) Lee, E. H. Iron oxide catalysts for dehydrogenation of ethylbenzene in the presence of steam. *Catal. Rev.* **1973**, *8*, 285−305.

(13) Afanas'ev, A. D.; Buyanov, R. A.; Chesnokov, V. V. Effect of water vapor on coking of iron oxides. *Kinet. Katal.* **1982**, *23* (5), 750−757.

(14) Babenko, V. S.; Buyanov, R. A. Spontaneous regeneration of iron potassium oxide catalysts in the presence of water vapor. *Kinet. Katal.* **1986**, *27* (2), 509−513.

(15) Babenko, V. S.; Buyanov, R. A.; Afanas'ev, A. D. Burnoff of carbonaceous deposits on potassium-promoted iron oxide catalyst. *Kinet. Katal.* **1982**, *23* (1), 131−137.

(16) Babenko, V. S.; Buyanov, R. A.; Afanas'ev, A. D. Burnout of carbon deposits from iron oxide catalyst promoted by alkali metals. (Translated) *Kinet. Katal.* **1982**, *23* (4), 977−982.

(17) Hirano, T. Roles of potassium-promoted iron oxide catalyst for dehydrogenation of ethylbenzene. *Appl. Catal*. **1986**, *26*, 65−79.

(18) Coulter, K.; Goodman, D. W. Kinetics of the dehydrogenation of ethylbenzene to styrene over unpromoted and K-promoted model iron oxide catalysts. *Catal. Lett*. **1995**, *31*, 1−8.

(19) Addiego, W. P.; Estrada, C. A.; Goodman D. W.; Rosynek M. P and Windham, R. G. An infrared study of the dehydration of ethylbenzene to styrene over iron based catalysts, *J. Catal*. **1994**, *146*, 407−414.

(20) Ketteler, G.; Ranke, W.; Schlögl, R. Potassium-promoted iron oxide model catalyst films for the dehydrogenation of ethylbenzene: an example for complex model systems. *J. Catal*. **2002**, *212*, 104−111.

(21) Muhler, M.; Schutze, J.; Wesemann, M.; Rayment, T.; Dent, A.; Schlogl, R.; Ertl, G. The nature of the iron oxide based catalyst for the dehydrogenation of ethlybenzene to styrene1. solid state chemistry and bulk characterization. *J. Catal*. **1990**, *126*, 339−360.

(22) Muhler, M.; Schlögl, R.; Reller, A.; Ertl, G. The nature of the active phase of the fe/k-catalyst for dehydrogenation of ethlybenzene. *Catal. Lett*. **1990**, *2*, 201−210.

(23) Kortaba, A.; Kruk, I.; Sojka, Z. Energetics of potassium loss from styrene catalyst model components: reassignment of k storage and release phases. *J. Catal*. **2002**, *211*, 265−272.

(24) Shekhah, O.; Ranke, W.; Schüle, A.; Kolios, G.; Schögl, R. Styrene synthesis: high conversion over unpromoted iron oxide catalysts under practical working conditions. *Angew. Chem., Int. Ed*. **2003**, *42*, 5760−5763.

(25) McKewan, W. M. Reduction kinetics of hematite in hydrogen-water vapor-nitrogen mixtures. *Trans. Metall. Soc. AIME* **1962**, *224*, 2−5.

(26) McKewan, W. M. Reduction of magnetite in H_2-H_2O-N_2 mixtures. *Trans. Metall. Soc. AIME* **1961**, *221*, 140−145.

(27) Quets, J. M.; Wadsworth, M. E.; Lewis, J. R. Kinetics of reduction of magnetite to iron and wustite in hydrogen-water vapor mixtures. *Trans. Metall. Soc. AIME* **1961**, *221*, 1186−1193.

(28) Tenenbaum, M.; Joseph, T. L. Reduction of iron ores under pressure by hydrogen. *Detroit Meet. Member AIME* **1938**, 59−73.

(29) Hayes, P. The effects of adsorbed oxygen on the kinetics of chemical reactions on metal surfaces. *Metall. Trans. B* **1979**, *10B*, 489−496.

(30) Landler, P. F. J.; Komarek, K. L. Reduction of wustite within the wustite phase in H_2-H_2O mixtures. *Trans. Metall. Soc. AIME* **1966**, *138*, 138−149.

(31) Lecznar, F. Transformation of hematite (α-Fe_2O_3) into ferromagnetic iron oxide (γ-Fe_2O_3). *Acta Technol. Acad. Sci. Hung.* **1957**, *16*, 383−398.

(32) Aharoni, A.; Frei, E. H.; Scheiber, M. Some properties of γ-Fe_2O_3 obtained by hydrogen reduction of α-Fe_2O_3. *J. Phys. Chem. Solids* **1962**, *23*, 545−554.

(33) Klug, H. P.; Alexander, L. E. *X-ray Diffraction Procedures: For Polycrystalline and Amorphous Materials*; John Wiley & Sons: New York, 1954; pp 410−416.

(34) Cullity, B. D.; Stock, S. R. *Elements of X-ray Diffraction*; Prentice Hall: Upper Saddle River, NJ, 2001; pp 347−361 and 275−294.

(35) Bish, D. L.; Howard, S. A. Quantitative phase analysis using the Rietveld methodol. *J. Appl. Crystallogr*. **1988**, *21*, 86−91.

(36) Mansker, L. D.; Jin, Y.; Bukur, D. B.; Datye, A. Characterization of slurry phase iron catalysts for Fischer−Tropsch synthesis. *Appl. Catal., A* **1999**, *186*, 277−296.

(37) Klug, H. P.; Alexander, L. E. *X-ray Diffraction Procedures: For Polycrystalline and Amorphous Materials*; John Wiley & Sons: New York, 1978.

(38) Ndlela, S. C. The role of reduction in the deactivation of potassium-promoted iron oxide dehydrogenation catalysts, Dissertation, Iowa State University, 2004.

(39) Plyasova, M.; Andrushkevich, M. M.; Kotel'nikov, G. R.; Buyanov, A.; Khramova, G. A.; Kustova, G. N.; Villert, M. V. Phase composition of an iron-chromium-potassium catalyst for the dehydrogenation of olefins I. *Kinet. Katal.* **1976**, *3*, 750−757.

(40) Plyasova, M.; Andrushkevich, M. M.; Kotel'nikov, G. R.; Buyanov, R. A.; Khramova, G. A.; Kusova, G. N.; Villert, M. V. Phase composition of an iron−chromium−potassium catalyst for the dehydrogenation of *n*-butylenes II. *Kinet. Katal.* **1976**, *5*, 1295−1302.

(41) Andrushkevich, M. M.; Plyasova, M.; Molchanov, V. V.; Buyanov, R. A.; Kotel'nikov, G. R.; Abramov, V. K. Characteristics of phase composition of iron/chromium/potassium catalyst under conditions of *n*-butene dehydrogenation. *Kinet. Katal.* **1978**, *2*, 422−427.

Received for review April 25, 2006
Revised manuscript received July 10, 2006
Accepted August 21, 2006

IE0605229